

EUMETSAT/ECMWF Fellowship Programme
Research Report No. 37

An evaluation of FY-3C MWHS-2 at ECMWF

Heather Lawrence, Niels Bormann, Qifeng Lu,
Alan Geer and Stephen English

June 2015

Series: EUMETSAT/ECMWF Fellowship Programme Research Reports

A full list of ECMWF Publications can be found on our web site under:

<http://www.ecmwf.int/en/research/publications>

Contact: library@ecmwf.int

©Copyright 2015

European Centre for Medium Range Weather Forecasts
Shinfield Park, Reading, RG2 9AX, England

Literary and scientific copyrights belong to ECMWF and are reserved in all countries. This publication is not to be reprinted or translated in whole or in part without the written permission of the Director-General. Appropriate non-commercial use will normally be granted under the condition that reference is made to ECMWF.

The information within this publication is given in good faith and considered to be true, but ECMWF accepts no liability for error, omission and for loss or damage arising from its use.

Abstract

This report presents an evaluation of the quality of data from the MicroWave Humidity Sounder 2 (MWHS-2) instrument which is flown on-board the China Meteorological Administration (CMA)'s Feng Yun (FY)-3C polar orbiting satellite. This instrument has humidity sounding channels in the 183 GHz band, similar to MHS and ATMS, and new temperature sounding channels at 118 GHz. These latter channels have not been flown on a space-borne instrument before and provide an interesting new source of information. In particular they are expected to be sensitive to temperature and cloud.

The data quality of MWHS-2 is evaluated for both 183 GHz and 118 GHz channels by firstly comparing observations to background radiances simulated from the ECMWF short-range forecasts. Secondly these values are compared to those from similar instruments. Finally results of experiments assimilating the 183 GHz channels in all-sky over a period of close to 6 months are presented.

Results show that the 183 GHz channels of MWHS-2 are comparable to equivalent channels on ATMS and MHS, both in terms of mean observation minus background and standard deviation of observation minus background, which is indicative of similar instrument biases and noise. Furthermore results of assimilation trials for these channels show a small positive impact on short-range humidity forecasts, which is further evidence of the good quality of the data. The 118 GHz channels have global biases similar to temperature sounding channels on AMSU-A and ATMS, in most cases. The standard deviation of clear-sky observation minus background departures for MWHS-2 118 GHz channels is higher than AMSU-A or ATMS temperature sounding channels, but close to the post-launch estimated noise of the MWHS-2 instrument. Striping can also be observed in maps of observation minus background for the higher peaking 118 GHz channels.

1 Introduction

The China Meteorological Administration (CMA)'s Feng Yun (FY)-3 polar orbiting satellite series carries microwave and infra-red instruments which provide vertical information on atmospheric temperature and water vapour. The series began with the launch of the first satellite, FY-3A, in May 2008 and continued with the launch of FY-3B in November 2012 and FY-3C, in September 2013. FY-3A and B were deemed research missions and the instruments flown onboard that are of particular interest for Numerical Weather Prediction (NWP) include the MicroWave Temperature Sounder (MWTS), MicroWave Humidity Sounder (MWHS), MicroWave Radiation Imager (MWRI) and the Infra-Red Atmospheric Sounder (IRAS). These instruments are similar to respectively MSU, MHS, AMSR-E and HIRS. FY-3C has MWRI and IRAS instruments but also carries updated versions of MWTS and MWHS, known as MWTS-2 and MWHS-2, which have more channels, and carries in addition a new GPSRO instrument, the GNSS radio-occultation sounder (GNOS), amongst other instruments.

The instruments aboard the FY-3 series bring additional information on the state of the atmosphere and are expected to provide an important contribution to NWP. Therefore a detailed assessment of the data quality is ongoing at ECMWF and other NWP centres. [Lu et al. \(2011a\)](#) and [Lu et al. \(2011b\)](#) assessed the microwave temperature sounder, MWTS, aboard the FY-3A and FY-3B satellites by comparing observations to the short-range ECMWF forecasts. Significant biases were found and it was suggested that these were related to shifts in frequency of the channel passbands, as well as to radiometer non-linearity. After correcting these issues the data quality of MWTS was found to be broadly comparable to that of AMSU-A ([Zhou et al., 2011](#)). [Chen et al. \(2014\)](#) recently assessed the impact of assimilating the MWHS instrument aboard the FY-3A and FY-3B satellites and found that the use of these data improved the fit of short-range forecasts to other observations, notably MHS, and slightly improved the short-range forecast scores when verified against analysis. As a result, the FY-3B MWHS instrument is now actively assimilated at ECMWF, as of September 2014.

Since the launch of FY-3C attention has turned to the instruments aboard this satellite. This report focuses on

the MWHS-2 instrument, presenting work done to assess the quality of the data. Like other microwave humidity sounders, including ATMS, MHS and MWHS, the MWHS-2 instrument has humidity-sounding channels around the 183 GHz water vapour band and window channels at frequencies close to 90 GHz and 150 GHz. In addition, MWHS-2 has 8 new sounding channels around the 118 GHz oxygen band. These latter channels have not been flown on a space-borne instrument before and thus provide an interesting source of new information. They are expected to be sensitive to temperature and cloud, similar to AMSU-A temperature sounding channels in the 50 - 60 GHz oxygen band. However, the temperature information is expected to be noisier than AMSU-A due to narrower bandwidths for these channels, which are necessary since at 118 GHz we are sampling the wings of a spectral line whereas for the AMSU-A channels around 50 - 60 GHz we are sampling between lines. On the other hand, a higher sensitivity to cloud and precipitation is expected at 118 GHz and a theoretical study by [Di Michele and Bauer \(2005\)](#) indicated that these frequencies were amongst those most suitable for retrievals of rain over oceans and snow over land and oceans.

In this study we present firstly an evaluation of FY-3C MWHS-2 observations against an NWP short-range forecast, a method that has become an integral part of calibration/validation exercises for new satellite data. The errors in short-range forecasts are, on average, of the order 0.1 K for tropospheric temperature sounding channels and of the order 1 K for microwave humidity sounding channels, in radiance space. These low errors make the model background a powerful tool for assessing the quality of observations, and such assessments have been done previously for a variety of atmospheric sounding and imaging instruments (e.g. [Bell et al., 2008](#), [Bormann et al., 2013](#), [Lu et al., 2011a,b](#)). Strong biases which could be detrimental to the assimilation of the data are usually visible in maps of observation minus background. Such biases were observed for SSMI/S (e.g. [Bell et al., 2008](#), [Geer et al., 2010](#)), and diagnosed to be related to solar intrusions into the warm calibration load and emission from the main reflector of the instrument.

Secondly we compare the background departure statistics for MWHS-2 to those of similar instruments. This allows us to compare the quality of the data to those of instruments which are actively assimilated at ECMWF. The standard deviation of observation minus background in particular is directly related to the instrument noise, errors in the background, representivity errors and errors in the radiative transfer forward model (used to transform atmospheric model variables to radiance space). Comparing values of standard deviation of observation minus background between similar instruments, with similar model background, representivity and radiative transfer errors, can provide a direct comparison of how noisy the data are in relation to other instruments. For the 183 GHz sounding channels we compared to equivalent channels on ATMS and MHS in clear-sky conditions. For the new 118 GHz sounding channels we could not compare to an instrument with measurements at the same frequencies. Instead, we selected temperature channels from AMSU-A and ATMS with similar weighting functions for comparison.

Finally we present results of assimilation trials that were carried out for a period of close to 6 months, assimilating the MWHS-2 183 GHz channels in the all-sky system. This assimilation was done in the same way as the operational all-sky assimilation of MHS (cycle 41R1 of the ECMWF model), in order to assess directly the quality of the data by evaluating whether it can be successfully assimilated in the same way as a similar instrument, and to assess the impact of these MWHS-2 183 GHz channels in the full ECMWF observing system.

The report is structured as follows. Firstly, the FY-3C MWHS-2 instrument and dataset used are described in section 2. Secondly in section 3 the observation minus background calculations for MWHS-2, ATMS, MHS and AMSU-A are described. Then in section 4 the methods for identifying cloud-affected data for the different instruments are described. The evaluations of observation minus background values and comparisons to other instruments are presented in section 5 for the 183 GHz channels and in section 6 for the 118 GHz channels. Finally the assimilation trials for the 183 GHz channels are presented in section 7.

2 FY-3C MWHS-2

The FY-3C satellite is polar orbiting with an equatorial crossing time of 10:00 (descending) and carries the Microwave Humidity Sounder -2 (MWHS-2), also known as the MicroWave Humidity and Temperature sounder (MWHTS), amongst other instruments. The full list of channels and their frequencies is given in Table 1, with equivalent channels for ATMS and MHS also shown. The number of fields of view, swath width and horizontal resolution for MWHS-2, ATMS and MHS are given in Table 2. MWHS-2 has a wider swath than MHS and ATMS, more fields of view and the same horizontal resolution for the 183 GHz sounding channels. For the window channels the horizontal resolution is slightly higher than ATMS at 89 GHz and the same as the ATMS equivalent channel at 150 GHz.

Channel Number			Central Frequency (GHz)		
MWHS-2	ATMS	MHS	MWHS-2	ATMS	MHS
1	16	1	89 (H)	88.2 (V)	89(V)
2	-	-	118.75 ± 0.08 (V)	-	-
3	-	-	118.75 ± 0.2 (V)	-	-
4	-	-	118.75 ± 0.3 (V)	-	-
5	-	-	118.75 ± 0.8 (V)	-	-
6	-	-	118.75 ± 1.1 (V)	-	-
7	-	-	118.75 ± 2.5 (V)	-	-
8	-	-	118.75 ± 3.0 (V)	-	-
9	-	-	118.75 ± 5.0 (V)	-	-
10	17	2	150 (H)	165.5 (H)	157 (V)
11	22	3	183 ± 1.0 (V)	183 ± 1.0 (H)	183 ± 1.0 (H)
12	21	-	183 ± 1.8 (V)	183 ± 1.8 (H)	-
13	20	4	183 ± 3.0 (V)	183 ± 3.0 (H)	183 ± 3.0 (H)
14	19	-	183 ± 4.5 (V)	183 ± 4.5 (H)	-
15	18	5	183 ± 7.0 (V)	183 ± 7.0 (H)	190.31 (V)

Table 1: MWHS-2 183 GHz and window channels, and equivalent ATMS and MHS Channel frequencies and polarisation at nadir

Instrument	Swath width	Channels	resolution	FOVs
MWHS-2	2660 km	1 - 9	29 km	98
MWHS-2	2660 km	10 - 15	16 km	98
ATMS	2580 km	3 - 16	32 km	96
ATMS	2580 km	17 - 22	16 km	96
MHS	2310 km	1 - 5	16 km	90

Table 2: MWHS-2 swath width, resolution and number of FOVs compared to ATMS and MHS

The 183 GHz channels are sensitive to humidity, both due to the water vapour band at 183 GHz and due to the water vapour continuum (see Fig. 1, shown courtesy of William Bell). They are also sensitive to cloud and precipitation, due to scattering from ice, rain and snow and the absorption and emission of cloud liquid water. The new 118 GHz channels are sensitive to temperature, and to cloud due to the absorption/emission of liquid water and the scattering of ice and precipitation. There is also some sensitivity to humidity for channels at the edges of the band due to the water vapour continuum, as can be seen by comparing the absorption

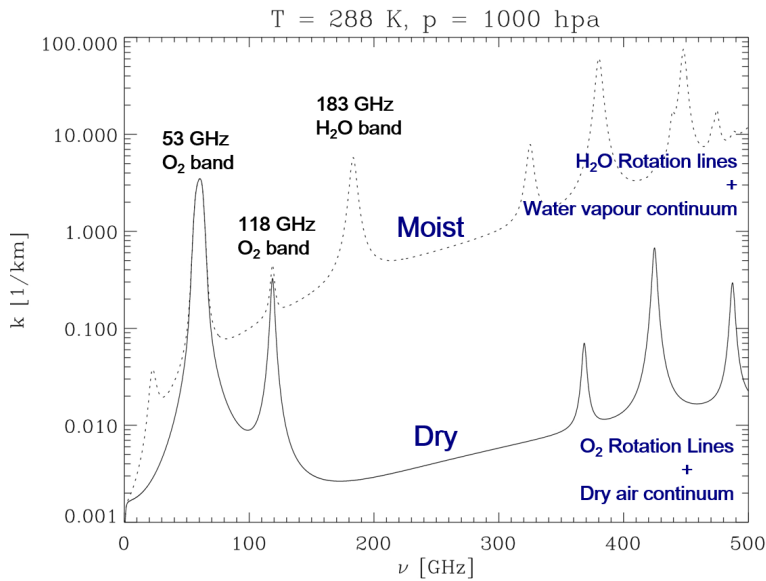


Figure 1: Figure, courtesy of William Bell, showing the absorption coefficient as a function of frequency in the microwave region, for a moist and dry atmosphere with a temperature of 288 K and a pressure of 1000hPa.

spectrum of a moist and a dry atmosphere, shown in Fig. 1. This is different to AMSU-A which has little to no humidity sensitivity. All MWHS-2 sounding channels are sensitive to different heights of the atmosphere. This is illustrated by Fig. 2 and Fig. 3, which show the clear-sky humidity and temperature Jacobians for the 183 GHz and 118 GHz channels respectively, normalised by the change in log pressure of each model level ($\Delta \ln p$). The clear-sky normalised temperature Jacobians of AMSU-A are also shown in Fig. 3 for reference. As these plots show, channels 2 - 4 of the 118 GHz sounding channels peak too high to be sensitive to cloud and water vapour and so they are expected to be purely temperature-sounding channels. The lower channels (5 - 7) on the other hand peak low enough to be sensitive to cloud. In addition channel 7 is sensitive to water vapour, as shown by the humidity Jacobian (with a weak sensitivity to water vapour for channels 5 and 6). Channels 8 and 9 are not plotted here since their weighting functions peak so low as to make them effectively imager channels.

In order to compare MWHS-2 118 GHz channels to AMSU-A and ATMS temperature sounding channels (in clear-sky conditions), we selected equivalent AMSU-A channel numbers based on the peak-height of their clear-sky Jacobians and their surface-to-space transmittance. These equivalent AMSU-A/MWHS-2 channel pairs are given in Table 3, along with their approximate peaking height and surface-to-space transmittance in clear-sky conditions. Note that the ATMS instrument has the same channels as AMSU-A but corresponding channels numbers are +1 higher than AMSU-A (ATMS channel 6 is equivalent to AMSU-A channel 5, etc.). The MWHS-2/AMSU-A channel pairs given in Table 3 are only approximately equivalent since the MWHS-2 weighting functions are broader than for AMSU-A. AMSU-A equivalent channels were selected for MWHS-2 channels 2 - 4 based on the peak heights of their Jacobians. For MWHS-2 channels 6 and 7 (the lowest peaking channels) equivalent AMSU-A channels were selected based on a similar surface-to-space transmittance.

For the study presented in this paper, a sample dataset was used for the period 1 June - 16 November 2014. It should be noted that improvements are still expected in the processing and understanding of the data, as a result of on-going calibration/validation activities at CMA and elsewhere, and some changes in data characteristics are therefore likely. Nevertheless, our analysis provides an initial assessment which forms the baseline for future data enhancements.

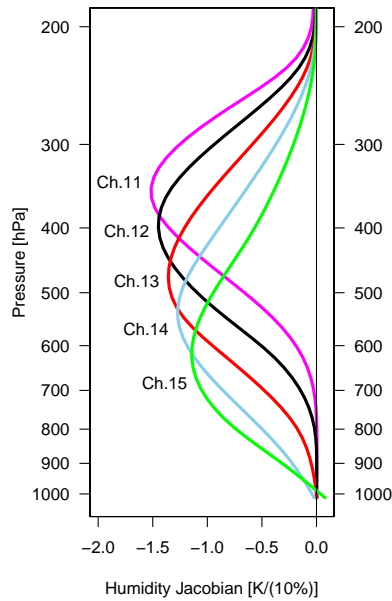


Figure 2: Clear-sky Humidity Jacobians for the MWHS-2 183 GHz channels (channels 11 - 15), normalised by the model level change in the log pressure ($\Delta \ln p$)

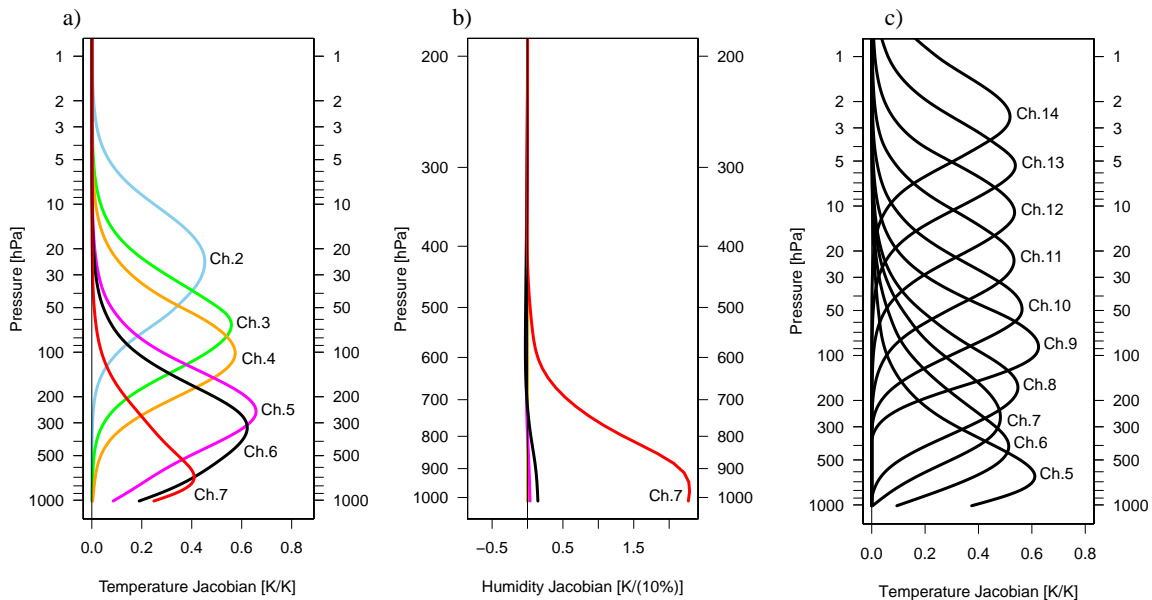


Figure 3: a) Clear-sky Temperature Jacobians for the 118 GHz channels, b) Clear-sky humidity Jacobians for the 118 GHz channels, and c) Clear-sky Temperature Jacobians for AMSU-A. All are normalised by the model level change in the log pressure ($\Delta \ln p$)

MWHS-2			AMSU-A		
Channel Number	Peak height	Surface-to-space transmittance	Channel Number	Peak height	Surface-to-space transmittance
2	20 hPa	0.000	11	20 hPa	0.000
3	60 hPa	0.000	10	50 hPa	0.000
4	100 hPa	0.000	9	90 hPa	0.000
5	250 hPa	0.013	7	300 hPa	0.001
6	300 hPa	0.036	6	400 hPa	0.011
7	700 hPa	0.233	4	-	0.243

Table 3: Comparable MWHS-2 118 GHz and AMSU-A channels and their approximate peaking height and average clear-sky surface to space transmittance over ocean.

3 Observation minus background calculations

First, we assess the quality of FY-3C MWHS-2 data by comparing observations to radiances simulated from the ECMWF 12-hour forecasts of atmospheric and surface variables, known as the background. Radiances simulated from the ECMWF model background are routinely calculated for all radiance observations used in the ECMWF assimilation system. This is done either in clear-sky conditions using the RTTOV forward model, or in all-sky conditions, using the RTTOV-SCATT forward model and including the forecast model cloud and precipitation fields. The former is used for instruments whose radiances are operationally assimilated in clear-sky conditions and the latter for microwave instruments whose radiances are operationally assimilated in all-sky conditions. For MWHS-2 we aim to assimilate the data in all-sky conditions, in order to exploit the cloud information as well as temperature and humidity information. This is consistent with MHS instruments, which are assimilated in all-sky conditions as of cycle 41R1 of the ECMWF model (Geer et al., 2014). Observation minus background values presented in this report were therefore calculated for both MWHS-2 and MHS using RTTOV-SCATT. At ECMWF, ATMS temperature and humidity sounding channels are still currently assimilated in clear-sky conditions, but work is ongoing to move the 183 GHz humidity sounding channels to all-sky assimilation. However, for the purposes of this study, an assimilation trial was run in which ATMS data were passively monitored, and the background in observation space for 183 GHz channels was calculated in all-sky using RTTOV-SCATT, in order to directly compare ATMS 183 GHz channels to MWHS-2 equivalent channels. Note that ATMS temperature channels were still calculated in clear-sky conditions. AMSU-A is operationally assimilated in clear-sky conditions, with simulated radiances calculated using RTTOV. However for some channels (channels 4 - 7), all-sky background radiances are also routinely calculated for thinned data over ocean only. For this study the observation minus background calculations for AMSU-A were calculated in all-sky for channels 4 - 7 and in clear-sky for channels 8 and higher (which have no cloud sensitivity).

For surface-sensitive channels the surface contribution in the background requires estimates of the surface emissivity and skin temperature. For the background calculations of microwave sounding instruments the skin temperature is taken from the ECMWF model background and the emissivity is calculated over ocean from the FASTEM v6 model and estimated over land and sea-ice from a combination of values retrieved from a window channel and dynamic emissivity atlases (see e.g. Geer et al., 2014, section 2.7). For the 183 GHz channels on MWHS-2, we chose to use the window channel close to 90 GHz for the emissivity retrieval over land and 150 GHz over sea-ice, as is done for MHS and the 183 GHz channels of ATMS. For the 118 GHz channels of MWHS-2 we used the same emissivity values over land as for the 183 GHz channels but over sea-ice we chose to use values retrieved from the 90 GHz channel instead of the 150 GHz channel. For AMSU-A and ATMS temperature sounding channels the 50.3 GHz window channel is used for surface emissivity retrieval.

The ECMWF bias correction scheme was applied to MWHS-2 data, and other instruments, and departure (observation minus background) statistics were calculated for observations both before and after bias correction. The bias correction is a variational bias correction scheme, known as VarBC (Dee, 2004, Auligné et al., 2007). In this scheme the bias of each channel of each instrument is modelled as a linear function of a set of predictors. The coefficients of these predictors are retrieved in the analysis with each cycle as additional control variables. VarBC is not applied to some conventional data or GPSRO data and these data act as an anchor to prevent the bias correction from removing model bias. VarBC is intended to remove biases due to forward model error and instrument calibration error and predictors are used because these errors can depend on the state of the atmosphere. The same predictors were used for MWHS-2 183 GHz channels as for MHS and ATMS, and 118 GHz channels as for AMSU-A.

4 Identifying cloud-affected data

For ATMS, MHS and MWHS-2, cloud-affected data can be identified using the scattering index (SI), which is calculated from observed values of the window channels on these instruments. The scattering index identifies areas of scattering from precipitation and cloud ice. It does not identify liquid water cloud, however, and so is only a partial filter. The SI can be calculated over land as the difference between the observations of the window channels close to 90 and 150 GHz (TB_{90} and TB_{150} respectively):

$$SI = TB_{90} - TB_{150}. \quad (1)$$

Over ocean an additional term removing the clear-sky background departures is usually included, in order to remove water vapour signatures:

$$SI = (TB_{90} - TB_{150}) - (TB_{90}^{clr} - TB_{150}^{clr}), \quad (2)$$

where TB_{90}^{clr} and TB_{150}^{clr} are the clear-sky background brightness temperatures of the 90 GHz and 150 GHz window channels. The ‘symmetric cloud predictor’ (C_{SYM}) is often used to identify areas where there is cloud in either the background or the observation (since in both cases the background departures are affected). It is calculated as:

$$C_{SYM} = (SI_{obs} + SI_{FG}) / 2, \quad (3)$$

where SI_{obs} is the observation scattering index and SI_{FG} is the background, or first guess, scattering index (Geer and Bauer, 2011, Geer et al., 2014). We found that filtering data with symmetric cloud predictors greater than 5 K, both over land and ocean, removed large negative values of background departures caused by cloud effects. For example Fig. 4 shows the background departures as a function of C_{SYM} for a 118 GHz and a 183 GHz channel of MWHS-2. The 183 GHz channel has lower background departures and is more affected by scattering than the 118 GHz channel, as we would expect. However in both cases a 5 K threshold removes most of the highly negative departures, while keeping approximately 70% of the data. It does not remove all of the ‘tail’ of negative departures however so this filter is only approximate. A lower threshold would remove more scattering-affected data but also removes a lot of data not affected by cloud. For example a threshold at 0 K would remove 90 % of the data for example and still not remove all of the negative ‘tail’. The threshold at 5 K was therefore chosen as a compromise.

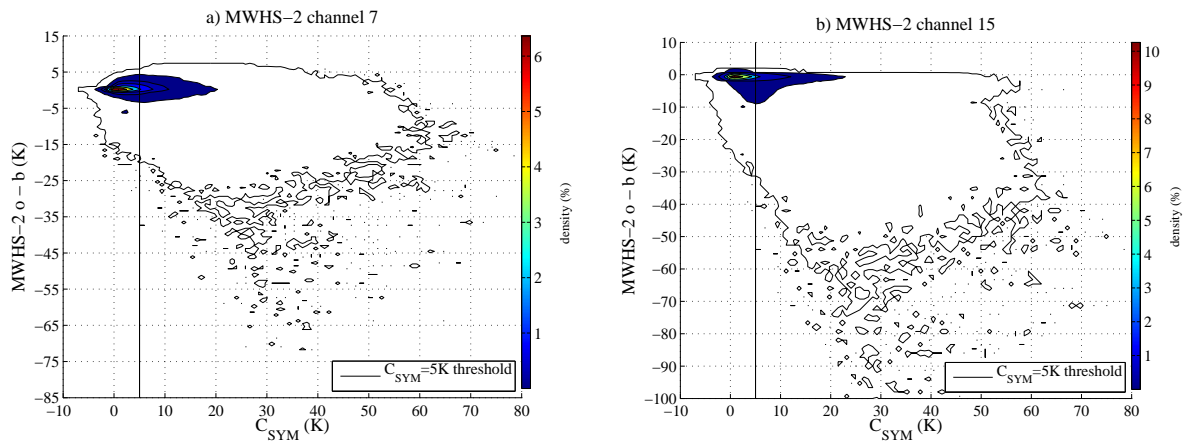


Figure 4: Background departures as a function of symmetric scatter index for 2 cycles of the ECMWF model (over a 24-hour period). Values are plotted for a) MWHS-2 channel 7 (a 118 GHz channel) and b) MWHS-2 channel 15 (a 183 GHz channel)

For AMSU-A we decided to use the method applied operationally for identifying cloud-affected scenes. Cloudy scenes were therefore identified using a combination of a background departure check for a window channel over land and ocean and a liquid water path check over ocean. Over land, data were identified as cloudy if the 50.3 GHz window channel background departures were larger than 0.7 K. Over ocean data were identified as cloudy if the liquid water path (calculated from window channel observations) exceeded 0.2 kg/m² or if the background departures of the 50.3 GHz window channel exceeded 3 K.

5 MWHS-2 183 GHz channels compared to the ECMWF background and MHS and ATMS

Maps of observation minus background (O - B) for MWHS-2 183 GHz channels for one cycle were compared to ATMS and MHS equivalent channels and these appear to be very similar. For example Fig. 5 shows a map of O - B before VarBC (but with the global mean bias removed) for MWHS-2 channel 13 and the equivalent map of ATMS channel 20 for 1 July 2014 (0z ECMWF model cycle). With the exception of Antarctica (where diurnal cycle model bias differences are likely to have an effect), the observed minus background brightness temperatures show very similar features. In both cases, observation minus background values are dominated by cloud and/or precipitation-affected data. For example, areas in the Tropics where red and blue points appear close to each other are likely to be an indication of displaced cloud, i.e. cloud is in a different location in the background and observations.

Timeseries (not shown) of background departures for MWHS-2 indicated that the departure statistics were stable over the test period for all MWHS-2 channels. We therefore compared the mean and standard deviation of MWHS-2 background departures for data over ocean after filtering for cloud, averaged over 1 month, to values for ATMS equivalent channels. Generally the mean background departures indicate biases either in the observations or the background and the standard deviation of background departures comprise instrument noise, forward model errors, representivity errors and background, or forecast model, errors. However forward model errors, representivity errors and background errors are similar between equivalent instruments and so comparing between MWHS-2 and ATMS or MHS gives us an indication of differences between the noise of the instruments. Values were calculated for clear-sky scenes over ocean only since the standard deviation of

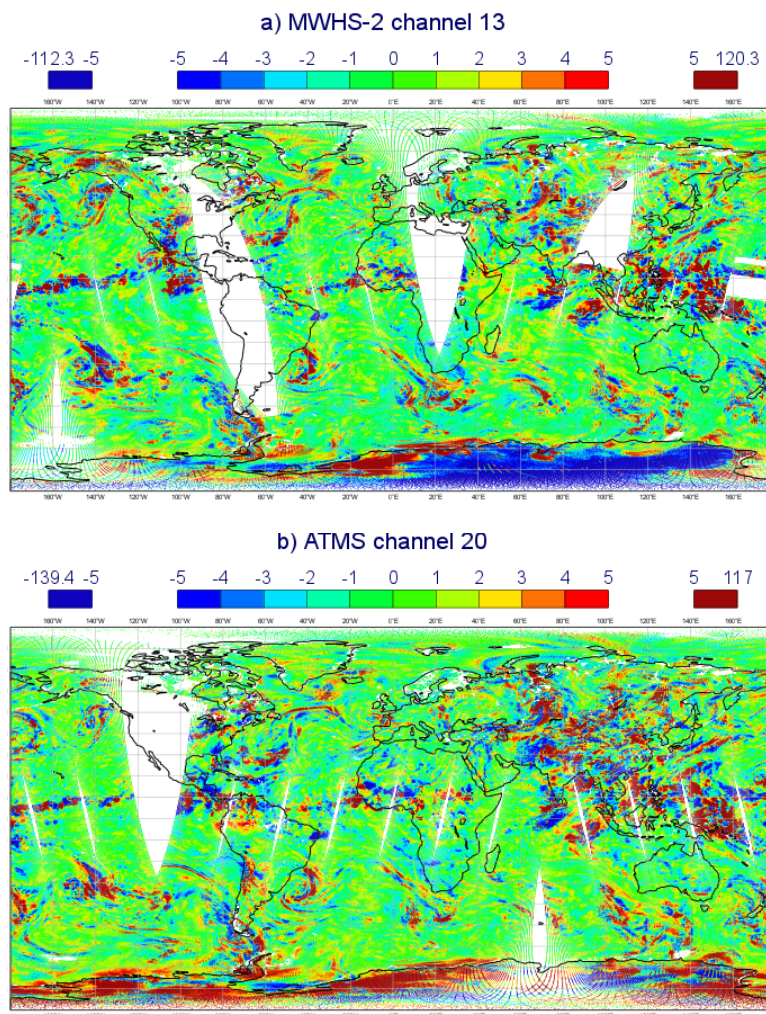


Figure 5: O - B minus global bias (excluding Antarctica) for one cycle (1 July 2014 0z) for a) MWHS-2 channel 13 and b) ATMS channel 20. All data before thinning is shown.

background departures is dominated by cloud in all data and the surface contribution to the forward model is more accurate over ocean than over land and sea-ice. The mean and standard deviations of background departures are shown in Fig. 6. Values are also shown for ATMS and MHS 183 GHz sounding channels and the window channels close to 90 GHz and 150 GHz, plotted against the equivalent MWHS-2 channel number.

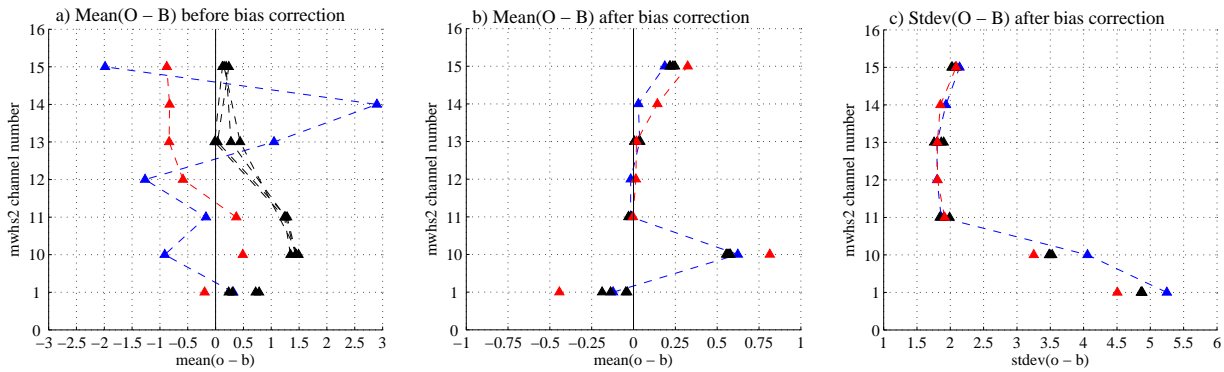


Figure 6: a) The monthly-averaged mean background departures for cloud-free data for MWHS-2 (blue), ATMS (red) and MHS (black) as a function of MWHS-2 channel number before bias correction over ocean, and b) after bias correction. c) The standard deviation of background departures for cloud-free data over ocean after bias correction.

Figure 6 shows that MWHS-2 has a higher magnitude of biases than ATMS, before bias correction is applied. The shape of biases is also different to MHS and ATMS. This is interesting since the bias shape of ATMS and MHS 183 GHz channels is thought to be related to humidity biases in the model, or biases in the spectroscopy, with a distinct vertical variation. Clearly MWHS-2 is showing a different pattern, indicating different instrument biases for MWHS-2. After bias correction these global biases are largely removed, as for ATMS and MHS (see Fig. 6b). The standard deviation of background departures for MWHS-2 are very similar to ATMS and MHS with values around 2.5 - 6 K for the 183 GHz channels. Only the window channels have slightly higher values. This is a good indication that the noise of MWHS-2 183 GHz sounding channels is comparable to MHS and ATMS.

The scan angle biases for the 183 GHz channels have a similar overall form to ATMS and MHS for most channels, as illustrated in Fig. 7 for data over ocean, after screening for cloud. There is a dip in bias in the first 5 scan angles for all channels, however, which is not seen for the MHS or ATMS instruments. This is likely to be instrument-related and in the assimilation trials for MWHS-2 the first 5 scan angles were therefore excluded. MWHS-2 also has more variability across the scan-line for all channels than is seen for ATMS, which has a smoother curve (see Fig. 7). However even for MWHS-2 this variation is small compared to the standard deviation of background departures. MWHS-2 channel 14 has a different scan-angle bias to its equivalent ATMS channel - see Fig. 7, which is likely to be an instrument-related difference. After bias correction the scan angle biases are smoothed to a straight line (not shown), although the small-scale variations have not been removed.

In summary, some differences have been observed in the biases for the 183 GHz MWHS-2 channels compared to ATMS and MHS. The global biases as a function of channel do not show the usual shape of MHS and ATMS, and the scan angle variation is not as smooth. The first 5 scan positions show a negative bias for most channels and should be blacklisted. These differences to ATMS and MHS indicate instrument biases for MWHS-2 and it would be useful to investigate this further and understand the sources. However the magnitude of the biases is not much larger than ATMS and MHS and VarBC is able to remove the majority of the bias (leaving only the small-scale scan-angle variation). The standard deviation of background departures for the MWHS-2 183 GHz channels is very similar to ATMS. This is encouraging and gives us the confidence to test the data in assimilation trials.

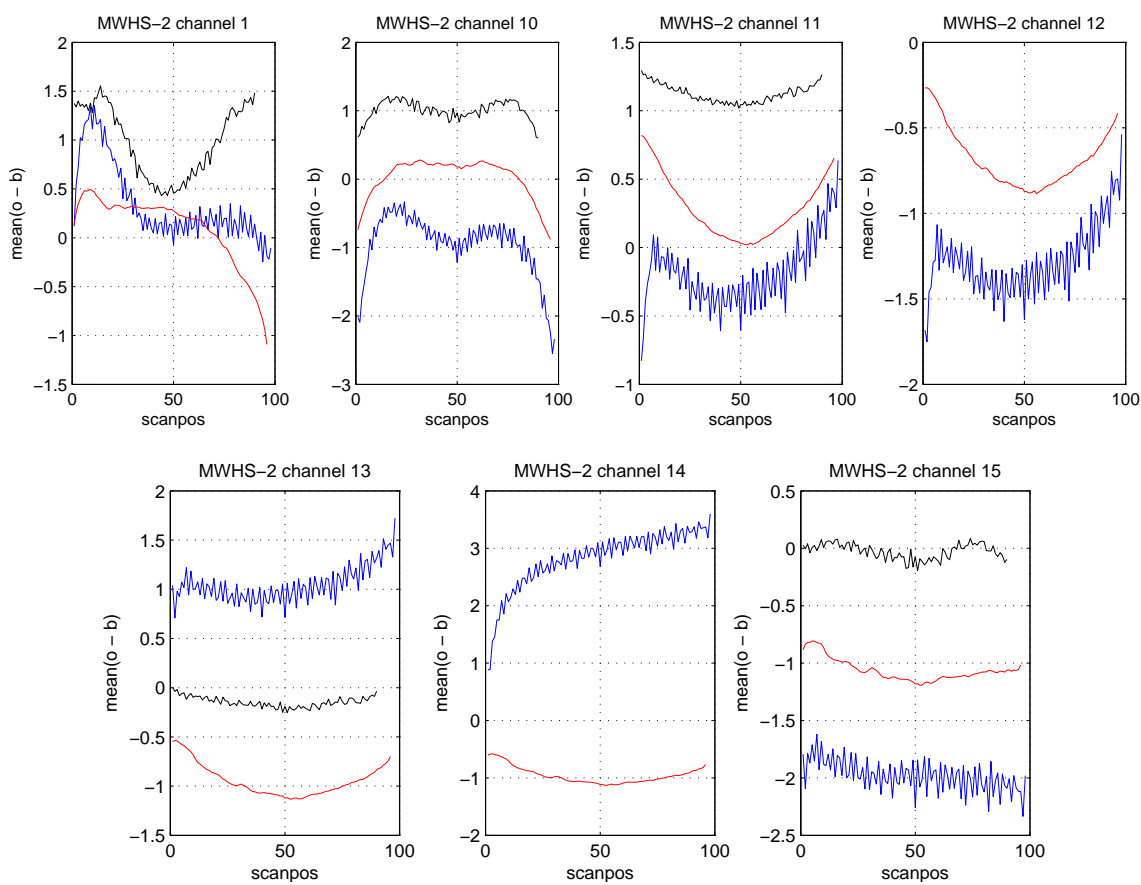


Figure 7: $\text{mean}(O - B)$ as a function of scan position for MWHS-2 (blue), and ATMS (red) and MetOp-B MHS (black) for equivalent channels, after cloud-screening.

6 MWHS-2 118 GHz channels compared to the ECMWF background and AMSU-A

In this section we analyse background departure (O - B) statistics for the 118 GHz MWHS-2 channels and compare these to AMSU-A and ATMS temperature sounding channels which peak at similar heights. The MWHS-2 and AMSU-A channel pairs for the comparison are given in Table 3. Maps of O - B for the 118 GHz channels show some striping visible for channels 2 - 6. This is shown in Fig. 8a for channel 3 and Fig. 9a for channel 6. A similar feature has been observed previously for ATMS temperature sounding channels (shown in Fig. 8c as well as Bormann et al., 2013). For ATMS, this is thought to result from $1/\text{frequency}$ or ‘flicker’ noise that is not captured by the calibration process.

Maps of background departures for channels 5 - 9 show a sensitivity to cloud effects for these channels, as expected. This can be seen in Fig. 9a for channel 6 and Fig. 10a for channel 7, for example. These cloud features are also visible for equivalent AMSU-A channels (also shown in the same figures), although these features are not so clearly visible in the maps of AMSU-A background departures due to the thinning. Some of the cloud and precipitation features seen in these channels are also visible in the MWHS-2 183 GHz channels (see Fig. 5 for example).

A 1 month mean and standard deviation of background departures was also calculated for the 118 GHz channels, after filtering for cloud, and these are shown in Fig. 11. For comparison the means and standard deviations of MetOp-B AMSU-A and ATMS for the same period are also shown. Note that the cloud screening is different for AMSU-A, ATMS and MWHS-2 which could affect biases for channels 6 and above of MWHS-2 and equivalent ATMS and AMSU-A channels. Also, the background for the ATMS temperature sounding channels were calculated for clear-sky conditions, whereas for AMSU-A channels 4 and 6 (shown against MWHS-2 channels 6 and 7) background values were calculated in all-sky. Biases were found to be of the order of 0.5 - 1 K for channels 5 - 9 and 2 K for channels 2 and 4. These biases are the same order of magnitude as AMSU-A and ATMS for most channels, with the exception of channels 2 and 4 of MWHS-2, which have higher biases. After bias correction most of these global biases are removed, as shown in Fig. 11b. Some bias remains for the lower peaking channels (6 - 9), but this is likely due to the presence of cloud which the filter has not been able to entirely remove, and is seen for the lower peaking 183 GHz channels on MWHS-2 and ATMS.

The standard deviation of background departures is higher for MWHS-2 channels than for AMSU-A or ATMS, as can be seen in Fig. 11c. The post-launch estimated noise is also plotted in this figure as the dashed blue lines (values from Nigel Atkinson, personal communication). Two lines are shown which indicate the Noise Equivalent delta Temperature (NEdT) estimated from the cold target (blue dashed line) and from the warm target (black dashed line). The NEdT varies between these values with scene temperature and so for Earth views it should be closer to the warm target than the cold target. The methods for calculating this noise account for both calibration noise and $1/\text{frequency}$ noise and so include the striping effects. For more information on how they are calculated see Atkinson (2014). The standard deviation of background departures for the higher-peaking MWHS-2 118 GHz channels is very close to the instrument noise. The lower peaking channels (channels 6 - 9) have higher standard deviation of background departures but this is likely due to cloud effects which have not been fully removed.

Plots of mean background departures as a function of scan angle for the 118 GHz channels showed the same small-scale variations and the ‘dip’ in background departures for the first 5 scan positions, as were seen for the 183 GHz channels. This can be seen in Fig. 12. For comparison, the scan-angle biases of MetOp-B AMSU-A and ATMS are also shown in this figure for the equivalent channels given in Table 3. Since AMSU-A scans approximately every 75 km and MWHS-2 every 27.5 km, the scan positions of AMSU-A have been multiplied by $75/27.5 = 2.7$ for comparison. The scan positions of AMSU-A and ATMS are also reversed in these figures,

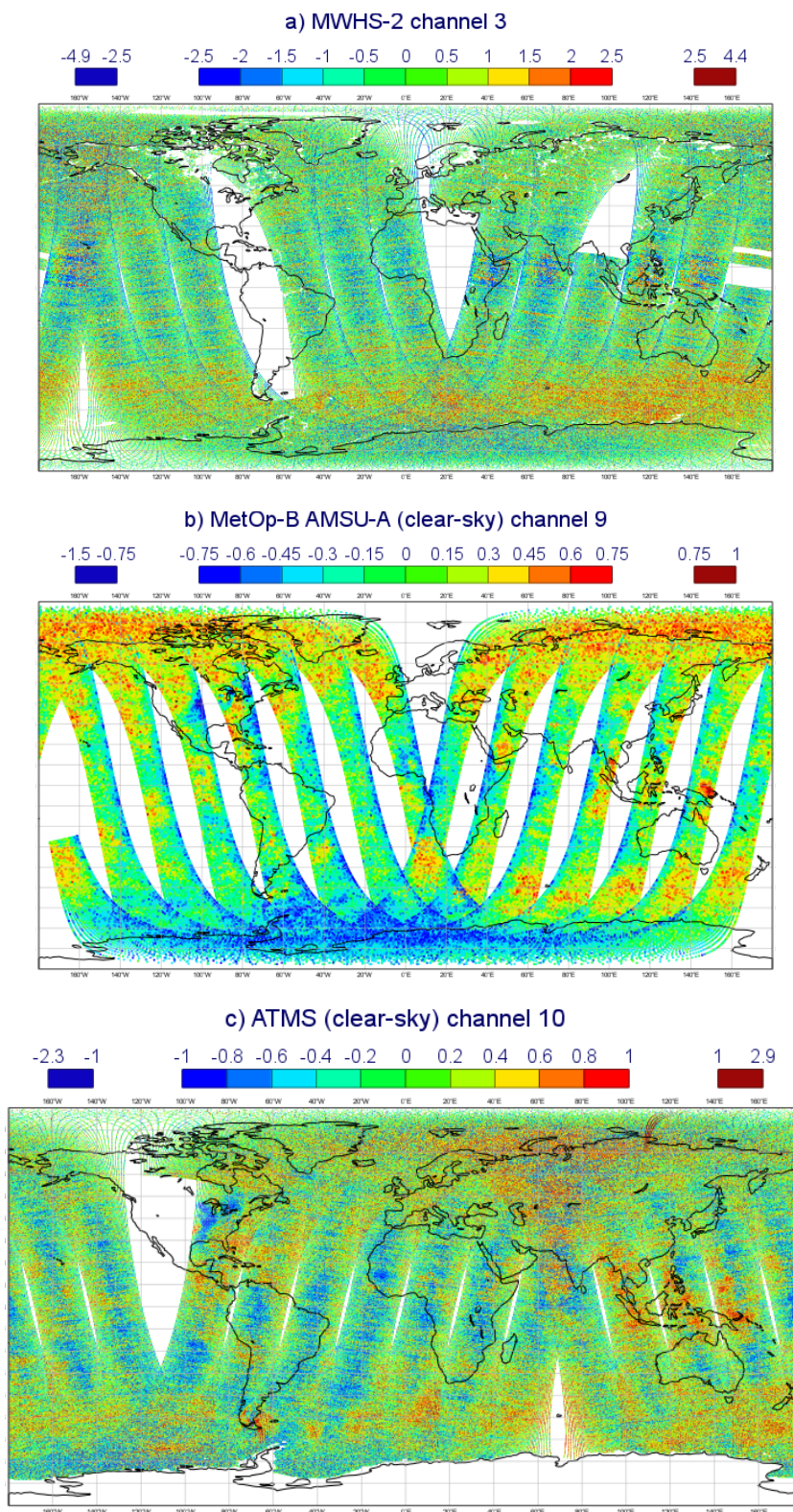


Figure 8: O - B minus global mean for one cycle (1 July 2014 0z) for a) MWHS-2 channel 3, b) MetOp-B AMSU-A channel 9 and c) ATMS channel 10. All data before thinning is shown.

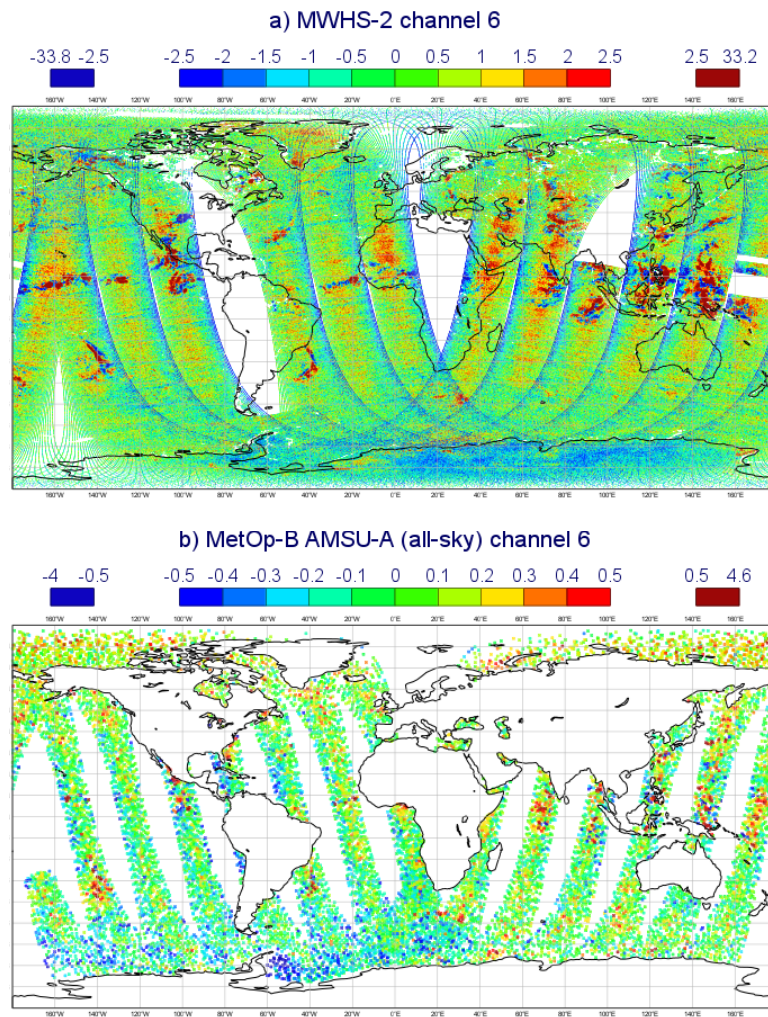


Figure 9: O - B minus the global mean (excluding Antarctica) for one cycle (1 July 2014 0z) for a) MWHS-2 channel 6, and b) MetOp-B AMSU-A channel 6. For MetOp-B AMSU-A data are shown after thinning for all-sky conditions (using RTTOV-SCATT) over ocean only. MWHS-2 data are showed before thinning.

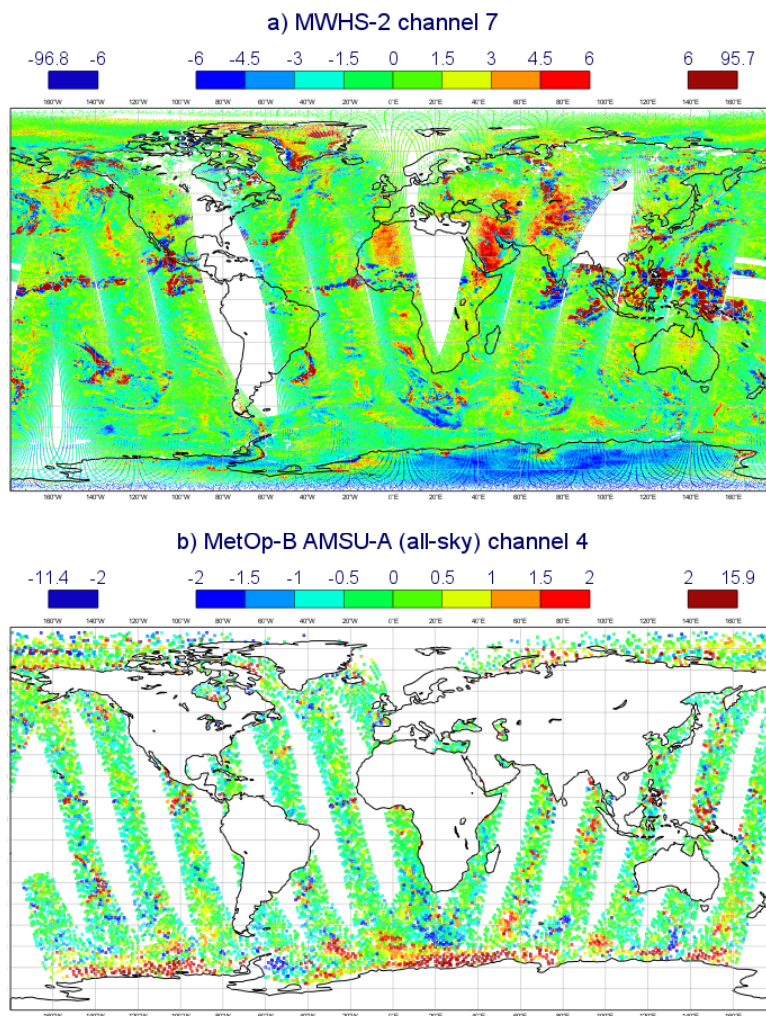


Figure 10: O - B minus the global mean (excluding Antarctica) before bias correction for one cycle (1 July 2014 0z) for a) MWHS-2 channel 7 and b) MetOp-B AMSU-A channel 4. For MetOp-B AMSU-A all data are shown after thinning with the background calculated in all-sky conditions, with RTTOV-SCATT.

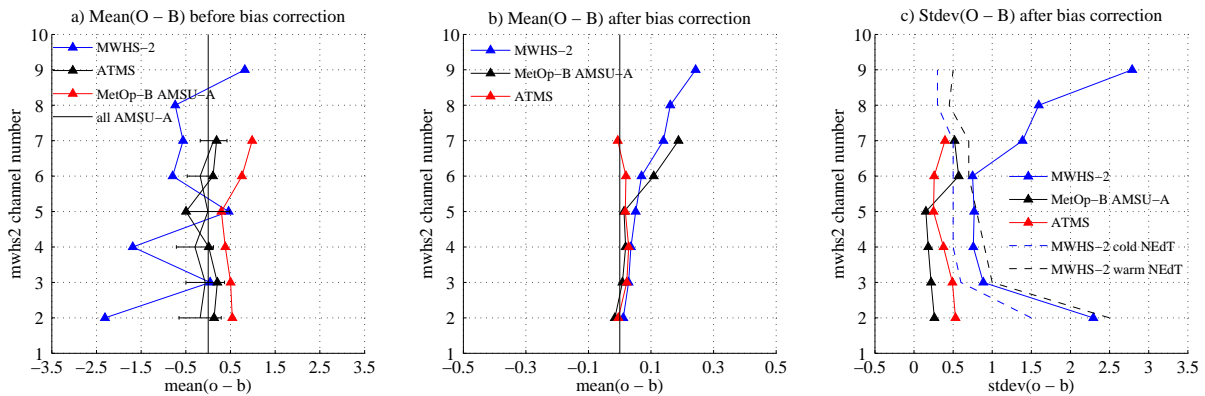


Figure 11: a) The monthly-averaged mean background departures after cloud-screening for MWHS-2 (blue) as a function of MWHS-2 channel number before bias correction over ocean, b) after bias correction over ocean. c) The standard deviation of cloud-screened background departures over ocean after bias correction. For reference the standard deviation of background departures for MetOp-B AMSU-A and the on-orbit NEdT for MWHS-2 calculated from the warm and cold targets are also shown.

to coincide with MWHS-2 angles (the AMSU-A and ATMS scan is done in a reverse sense to MWHS-2) and the first and last 3 scan positions are excluded for AMSU-A, as these are blacklisted operationally. In most cases the shape of the scan-angle biases for MWHS-2 is quite similar to AMSU-A and ATMS. Channels 2 - 6 also have relatively low scan angle bias (excepting the first 5 scan positions).

In summary, maps of observation minus background departures show striping in the higher-peaking 118 GHz sounding channels and strong cloud and precipitation effects for the lower peaking channels 5 - 7. The standard deviation of background departures is of the order of 0.9 K for channels 2 - 6, around 2.3 K for channel 2 and 1.5 K for channels 7 - 8. These values are higher than for AMSU-A or ATMS for equivalent temperature-sounding channels but are very close to the post-launch estimated instrument NEdT values. Biases of observation minus background have a similar order of magnitude between MWHS-2 and AMSU-A, with the exception of MWHS-2 channels 2 and 4 which have higher biases. Scan angle biases show the same variability and ‘dip’ for the first 5 scan positions as were seen in the 183 GHz channels, but otherwise have a similar shape to AMSU-A channels.

7 Testing the 183 GHz channels by assimilation in the full ECMWF observing system

7.1 Observation errors for the 183 GHz channels

In order to perform assimilation trials for the 183 GHz channels, observation errors must first be defined. For the all-sky assimilation of MHS and microwave imager instruments, observation errors are higher in regions where cloud is present in the background or the observations and lower in clear-sky regions (see Geer et al., 2014, Geer and Bauer, 2011, for example). This is done to account for representivity and model errors which are higher in the presence of cloud. For MHS, cloudy regions are defined using the symmetric cloud predictor (C_{SYM}), given by (3). Observation errors vary quadratically with C_{SYM} , starting at a minimum value, which is an estimate of clear-sky observation errors, and then increasing quadratically with C_{SYM} up to a saturation

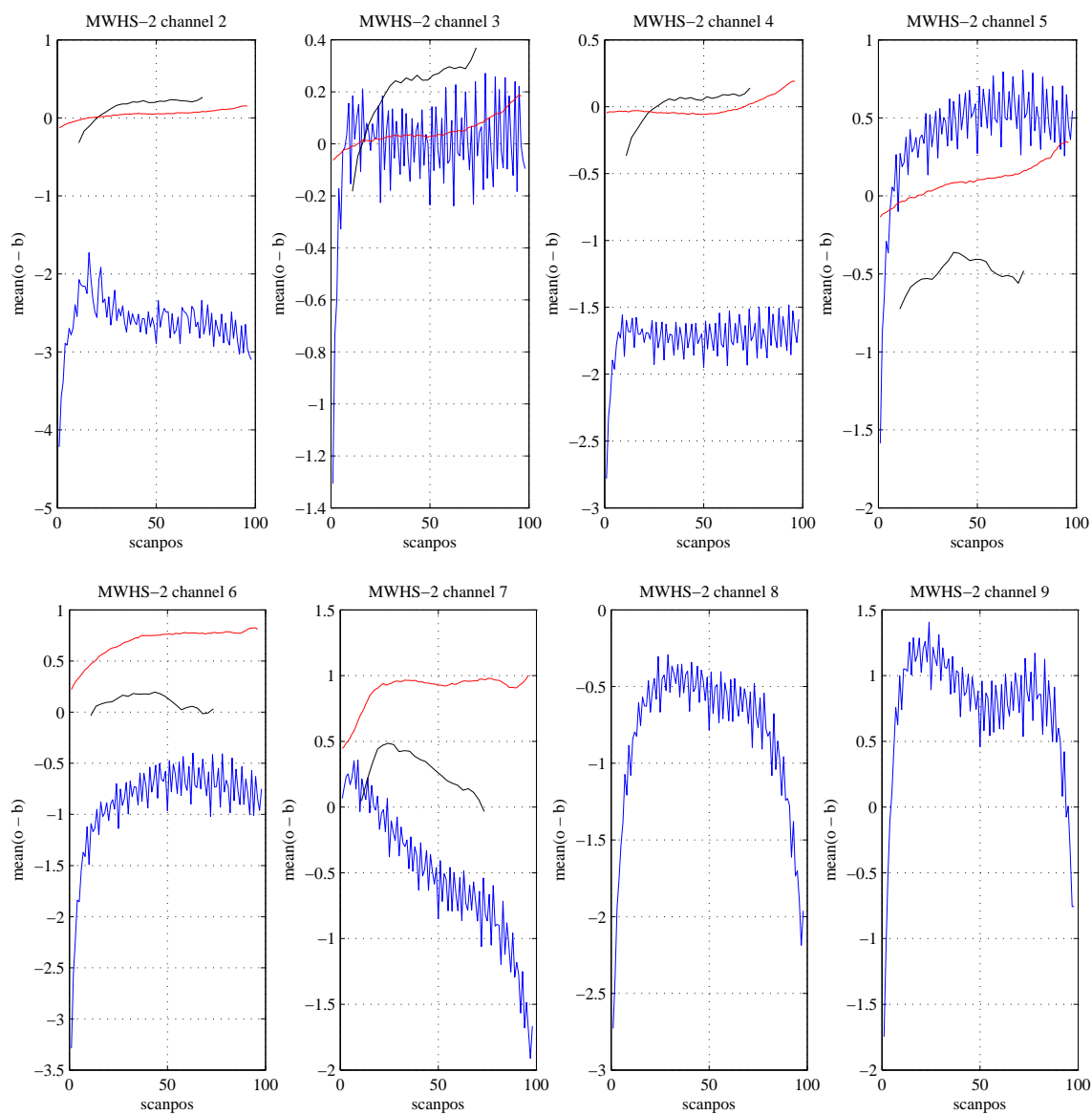


Figure 12: mean(O - B) as a function of scan position, after cloud-screening, for 118 GHz channels of MWHS-2 (blue), and ATMS (red) and MetOp-B AMSU-A (black) for equivalent channels.

point. Mathematically this is expressed as follows (Geer et al., 2014):

$$g(C_{SYM}) = \begin{cases} g_{clr}, & \in C_{SYM} \leq C_{clr} \\ g_{clr} + (g_{cld} - g_{clr}) \left(\frac{C_{SYM} - C_{clr}}{C_{cld} - C_{clr}} \right)^2, & \in C_{clr} < C_{SYM} < C_{cld} \\ g_{cld} & \in C_{SYM} \geq C_{cld} \end{cases} \quad (4)$$

where $g(C_{SYM})$ is the observation error, C_{clr} and C_{cld} are the clear and cloudy thresholds, g_{clr} is the minimum, clear-sky observation error and g_{cld} is the maximum, ‘cloudy’ observation error is g_{cld} . Different values of C_{clr} , C_{cld} , g_{clr} , and g_{cld} are used over land and ocean and no model is used over sea-ice - instead constant values are used (see Geer et al., 2014).

For MWHS-2 we adopted the same observation error model as for MHS for the equivalent channels and intermediate values for the two new channels. To check whether this was reasonable we calculated the standard deviation of background departures as a function of the symmetric cloud predictor for MWHS-2. These are plotted in Fig. 13 as the solid black lines. (Channel 11 has the lowest values, then channel 12 and so on up to channel 15 which has the highest values.) For comparison, values are also shown for MHS (blue lines) for equivalent channels. Over ocean the standard deviation of background departures has a similar slope for both MHS and MWHS-2 (for equivalent channels). However, for higher values of C_{SYM} we found the standard deviation of background departures continues increasing for MWHS-2 when MHS values had saturated. Therefore we decided to use the same observation error model for MWHS-2 as for MHS but extend the saturation point for MWHS-2. Over land there are some small differences in the slope of the lowest peaking MWHS-2 channel (channel 15) and the lowest peaking MHS channel (channel 5). However we decided to use the same observation error model as for MHS, extending the saturation points as over ocean. The observation errors adopted for each channel are shown as the black dashed lines in Fig. 13 and again the lower values correspond to channel 11, then channel 12 and so on. The observation errors have the same slope and minimum (clear-sky) values as those currently being tested for equivalent ATMS channels in the all-sky stream (saturation points are different). The values of C_{clr} , C_{cld} , g_{clr} and g_{cld} adopted for the different MWHS-2 183 GHz channels over land and ocean are given in Table 4.

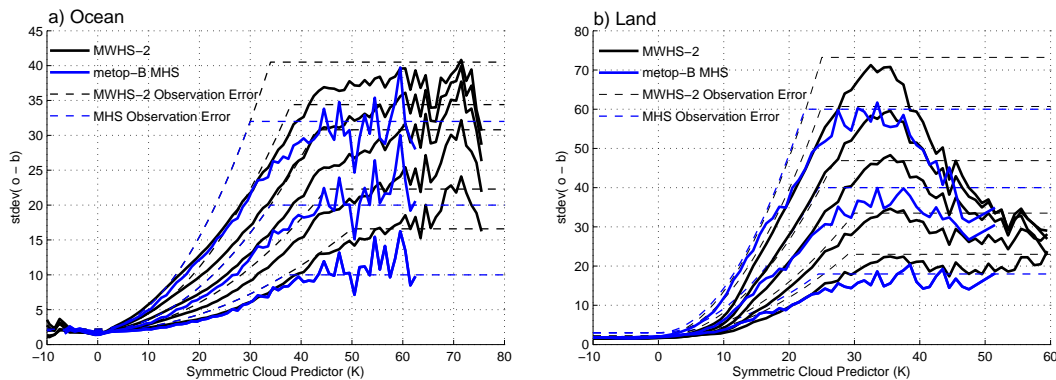


Figure 13: Observation error as a function of symmetric cloud predictor for channels 11 - 15 over ocean (a) and land (b). Values with number of data less than 20 are excluded.

	Channel	g_{ctr}	g_{cld}	C_{ctr}	C_{cld}
Ocean	11	2.0	16.6	0.0	50.0
	12	2.0	22.3	0.0	45.0
	13	2.0	30.8	0.0	43.0
	14	2.2	34.4	0.0	38.0
	15	2.2	40.5	0.0	34.0
Land	11	2.0	23.0	0.0	29.0
	12	2.0	33.5	0.0	30.0
	13	2.0	46.9	0.0	27.0
	14	2.2	60.7	0.0	25.0
	15	2.2	73.2	0.0	25.0

Table 4: Parameters for the observation error model for MWHS-2 183 GHz channels. All units are Kelvin.

7.2 Assimilation Trials

Assimilation trials were performed on almost 6 months of sample data for the period 5 June 2014 - 16 November 2014. These were done at a horizontal resolution of T511 (around 40 km), with 137 levels in the atmosphere and for a recent version of the ECMWF model (cycle 40r2 with additional contributions to cycle 41R1) which included the assimilation of MHS data in the all-sky stream, but kept the assimilation of the 183 GHz channels of ATMS in the clear-sky stream. The following assimilation trials were run:

- ‘Control’ - 40r2 with contributions to 41r1, including the full observing system
- ‘MWHS-2 full 183 GHz assimilation’ - channels 11 - 15 of MWHS-2 actively assimilated over land, ocean and sea-ice
- ‘MWHS-2 MHS-like assimilation’ - channels 11, 13, 15 only (equivalent to the 3 MHS channels) assimilated over land, ocean and sea-ice

Observation errors similar to MHS observation errors were used, as described in section 7.1, and the same orography and latitude screening was applied to MWHS-2 as for equivalent MHS channels. The orography and latitude screening for the two new MWHS-2 channels was done in the same manner as the MHS channels peaking just below, i.e. channel 14 MWHS-2 screening was the same as channel 5 MHS and channel 12 the same as channel 4 MHS. A latitude screening was applied to channels 14 and 15 where data for latitudes greater than 60°N or 60°S were not used, as is done for channel 5 of MHS. In addition a cold-air outbreak screening was applied (see [Lonitz and Geer, 2015](#)), as for MHS channel 5. Emissivity estimation was performed in the same way as MHS, as described in section 3. For further details on the all-sky assimilation of microwave humidity sounders see [Geer et al. \(2014\)](#).

7.3 Results

The impact on forecast accuracy of assimilating MWHS-2 183 GHz channels was assessed by analysing the change in fits of other observations to the background (short-range forecasts), as well as the change in forecasts minus analysis for forecast days 1 - 10. The former allows us to assess the impact on short-range forecasts and this analysis is presented in section 7.3.1. The latter allows us to assess the impact on longer-range forecasts and is presented in section 7.3.2.

7.3.1 Change in fits of observations to the analysis and short-range forecasts

The main changes from assimilating MWHS-2 183 GHz channels were seen in the fits of the background, or short-range forecast, to the water vapour channels of AIRS, IASI and HIRS and the humidity sounding channels of ATMS, MHS and SSMI/S. A reduction in background departures of around 0.5% was seen for these instruments, indicating an improvement in the short-range humidity forecast as a result of the assimilation of MWHS-2. This reduction in background departures is shown in Fig. 14 and Fig. 15. These changes were seen both when assimilating the full 5 channels and when assimilating 3 channels of MWHS-2. The background departures for ATMS appear to be further reduced when using 5 channels instead of 3.

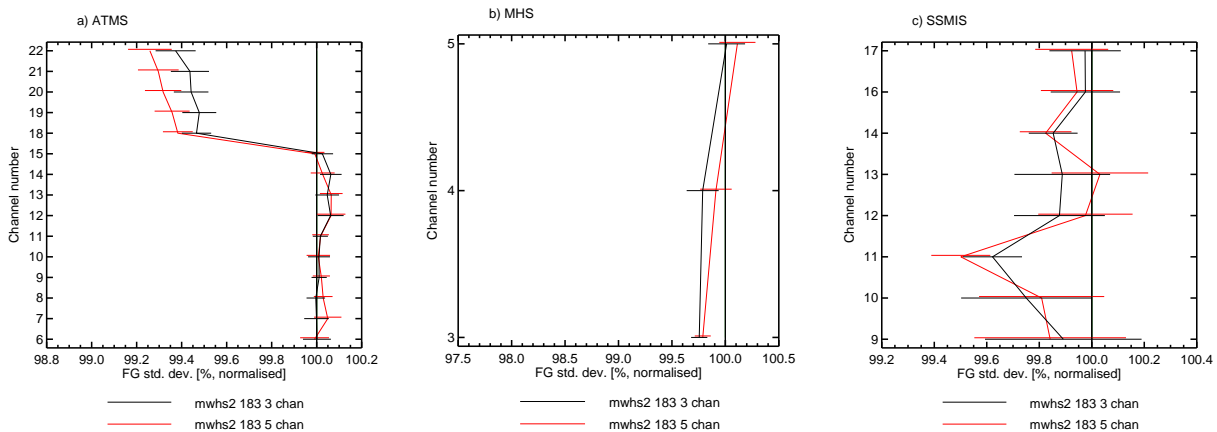


Figure 14: Standard deviation of background departures of (left-to-right) ATMS, MHS and SSMIS for the 5 channel and 3 channel experiments, averaged globally. Values are normalised by the control standard deviations of background departures and so values below 100 indicate an improved fit of the background to the observations.

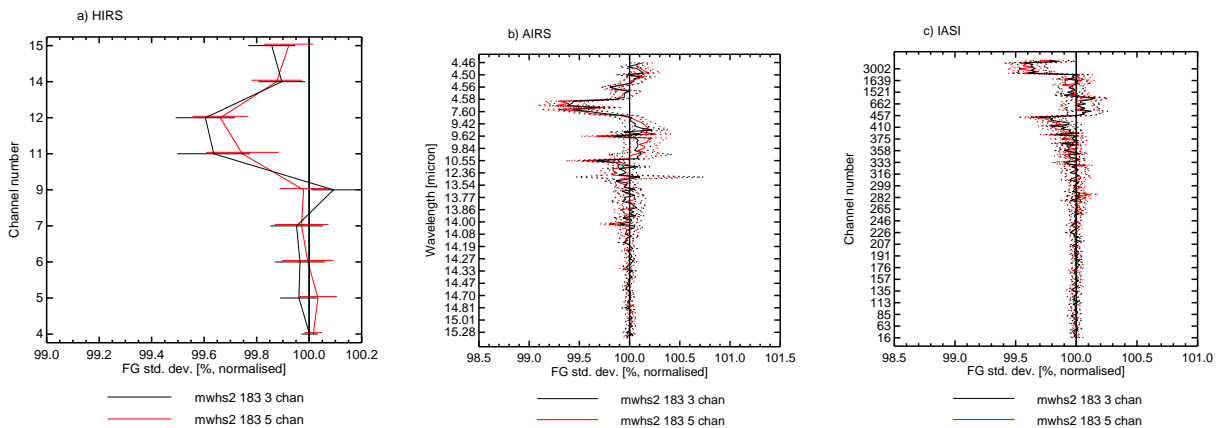


Figure 15: As Fig. 14 but values are shown for (left-to-right) HIRS, AIRS and IASI instruments.

7.3.2 Forecast scores

For both sets of experiments, the impact on forecast scores was fairly neutral overall. For example Fig. 16 shows the geopotential height at 500 hPa as a function of forecast day, averaged over the Northern and Southern Hemisphere extra-Tropics and 17 shows the same for vector wind and temperature in the Southern Hemisphere extra-Tropics, Tropics and Northern Hemisphere extra-Tropics.

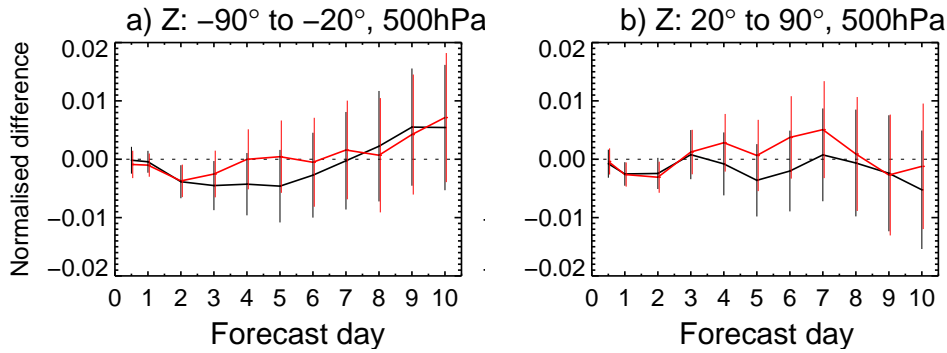


Figure 16: Change in standard deviation of geopotential height forecast minus analysis as a function of forecast day at 500hPa height, averaged over a) the Southern Hemisphere extra-tropics and b) the Northern Hemisphere extra-tropics. The red lines indicate the 5 channel experiment minus the control and the black lines the 3 channel experiment minus control. Error bars indicate statistical significance in the 95th percentile and values below zero indicate a forecast improvement compared to the control. Results are based on 338 - 357 cases covering 5 months and 17 days.

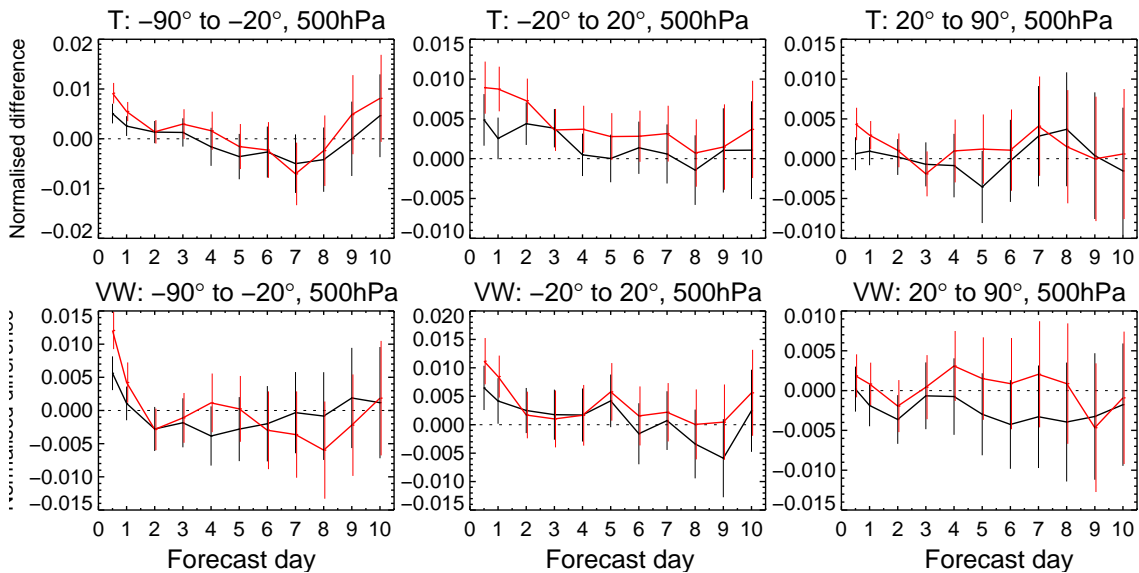


Figure 17: Change in standard deviation of temperature forecast minus analysis (top) and vector wind forecast minus analysis (bottom) as a function of forecast day, averaged over a) the Southern Hemisphere extra-tropics, b) the Tropics and c) and the Northern Hemisphere extra-tropics, all at 500 hPa height. The red lines indicate the 5 channel experiment minus the control and the black lines the 3 channel experiment minus control. Error bars indicate statistical significance in the 95th percentile and values below zero indicate a forecast improvement compared to the control. Results are based on 338 - 357 cases covering 5 months and 17 days.

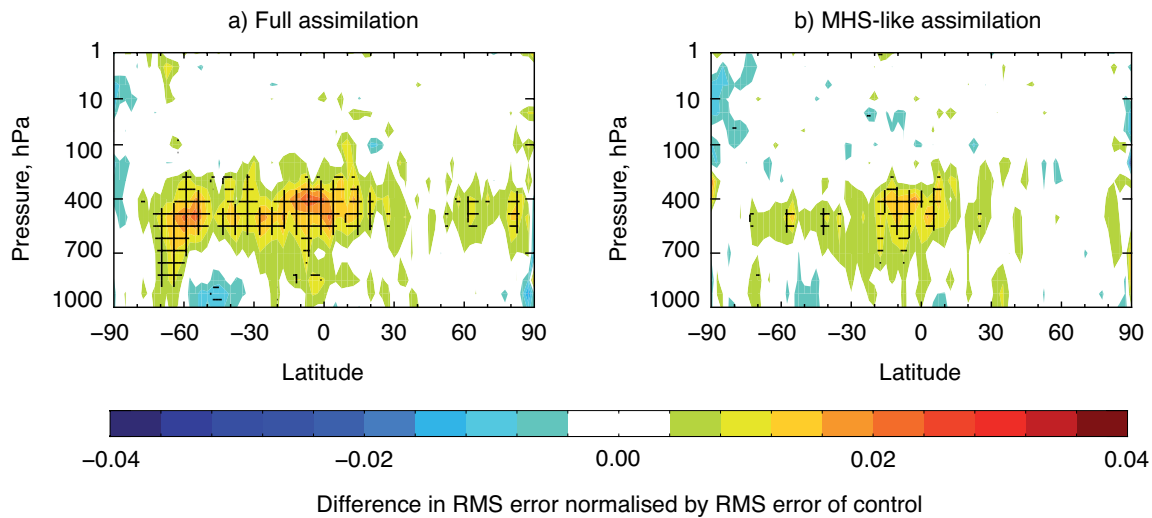


Figure 18: Change in the root mean square vector wind 12-hour forecast minus (own) analysis as a function of Latitude (x-axis) and Pressure (y-axis) for a) 'Full assimilation' experiment minus control and b) 'MHS-like assimilation' channel experiment minus control.

Some apparent degradations can be seen in the 12-hour forecast scores for vector wind and temperature, shown in Fig. 17. This can also be seen in the latitude-pressure plots of Fig. 18 for the 'Full assimilation' minus control experiments and the 'MHS-like assimilation' minus control experiments. Since forecast scores are calculated against own analyses the 12-hour forecast minus analysis values are indicative of larger increments. This increase in the increments could be due to a degradation in the accuracy of the short-range forecasts. Alternatively it could be due to a change in the analysis, with the introduction of new data making the analysis more variable. It could also be due to a forecast model bias which is effectively fighting with the observations. In this case an improvement in the analysis due to the observations would not translate into an improved forecast. A degradation in forecast accuracy seems unlikely, given the improvement in background departures of ATMS, MHS, AIRS and IASI. However, it is possible to have a degradation in the analysis and short-range forecasts at the resolution of the model, but an improvement at the satellite data resolution, which is coarser. Overall, this increase in increments warrants further investigation. It is also interesting to note that increments are larger when assimilating 5 channels compared to assimilating 3. A possible explanation is that we have not accounted for inter-channel error correlations which are stronger when using the full 5 channels, and in doing so we have limited the potential benefit of using 5 channels compared to 3. This could be investigated further in future work.

8 Conclusions

In conclusion, the quality of the MWHS-2 instrument was assessed by comparing observations to ECMWF background radiances and by comparing observation minus background values to similar instruments. The following was found:

- Mean observation minus background for 183 GHz channels are of a similar order of magnitude to MHS and ATMS but show a different vertical pattern. These global biases are successfully removed by VarBC.
- Standard deviations of observation minus background for the 183 GHz channels are comparable to ATMS and MHS, indicating a similar noise.

- Scan-angle biases show a small-scale variability for MWHS-2 183 GHz and 118 GHz channels which is not observed for other instruments.
- Maps of observation minus background departures for MWHS-2 118 GHz channels 2 - 6 show striping.
- Maps of observation minus background departures show the effects of cloud and precipitation for MWHS-2 lower-peaking 118 GHz channels 5 - 7.
- Monthly mean observation minus background departures show global biases of less than 1 K for most 118 GHz channels and a similar order of magnitude as AMSU-A. However global biases are close to 2 K for channels 2 and 4, which is higher than for AMSU-A instruments.
- Standard deviations of observation minus background departures for the 118 GHz channels in clear-sky conditions are higher than AMSU-A temperature sounding channels peaking at a similar height, but close to the post-launch estimated instrument NEdT values for MWHS-2 (which are higher than for AMSU-A or ATMS).

In order to further assess the quality of the MWHS-2 183 GHz channels, and to prepare for operational assimilation, assimilation trials were performed assimilating all 5 of the 183 GHz sounding channels globally ('full assimilation') as well as assimilating only 3 channels in an 'MHS-like' assimilation. In both cases assimilating the 183 GHz channels showed increased increments of vector wind, temperature and humidity, improved fits of the short-range forecasts to other humidity-sensitive instruments and neutral impact on forecast scores. The 'Full Assimilation' experiment showed increased increments compared to the 'MHS-like' assimilation and a small improvement in fits of short-range forecasts to ATMS 183 GHz channels. Assimilating 5 channels compared to 3 shows a small additional benefit for the short-range humidity forecast.

Acknowledgements

Heather Lawrence's work at ECMWF was funded by the EUMETSAT fellowship programme. Qifeng Lu's work at ECMWF was funded by the NWP-SAF visiting scientist programme and his work at CMA by the China Meteorological Administration Special Public Welfare Research Fund GYHY201206002. William Bell, Nigel Atkinson and Katie Lean are gratefully acknowledged for their contributions to this work.

References

- N. Atkinson. NEdT specification and monitoring for microwave sounders. *UKMO Satellite Applications Technical Memo*, 24, 2014.
- T. Auligné, A. McNally, and D.P. Dee. Adaptive bias correction for satellite data in a Numerical Weather Prediction system. *Q. J. R. Meteorol. Soc.*, 133:631–642, 2007.
- W. Bell, B. Candy, N. Atkinson, F. Hilton, N. Baker, N. Bormann, G. Kelly, M. Kazumori, W.F. Campbell, and S.D. Swadley. The assimilation of SSMIS radiances in numerical weather prediction models. *IEEE Trans. Geoscience. Rem. Sensing.*, 46:884 – 900, 2008.
- N. Bormann, A. Fouilloux, and W. Bell. Evaluation and assimilation of ATMS data in the ECMWF system. *J. Geophys. Res.*, 118:12970 – 12980, 2013.

- K. Chen, S. English, N. Bormann, and J. Zhu. Assessment of FY-3A and FY-3B MWHS observations. *ECMWF Tech. Memo.*, 734, 2014.
- D. Dee. Variational bias correction of radiance data in the ECMWF system. *Proceedings ECMWF Workshop on Assimilation of high spectral resolution sounders in NWP, 28 June - 1 July 2004*, 2004.
- S. Di Michele and P. Bauer. Passive microwave radiometer channel selection based on cloud and precipitation information content estimation. *ECMWF Tech. Memo.*, 475, 2005.
- A. Geer and P. Bauer. Observation errors in all-sky data assimilation. *Q. J. R. Meteorol. Soc.*, 137:2024–2037, 2011.
- A. Geer, F. Baordo, N. Bormann, and S. English. All-sky assimilation of microwave humidity sounders. *ECMWF Tech. Memo.*, 741, 2014.
- A.J. Geer, P. Bauer, and N. Bormann. Solar biases in microwave imager observations assimilated at ecmwf. *IEEE Trans. Geoscience. Rem. Sensing.*, 48:2660–2669, 2010.
- K. Lonitz and A. Geer. New screening of cold-air outbreak regions used in 4D-Var all-sky assimilation. *EU-METSAT/ECMWF Fellowship Programme Research Report*, 35, 2015.
- Q. Lu, W. Bell, P. Bauer, N. Bormann, and C. Peubey. Characterizing the FY-3A microwave temperature sounder using the ECMWF model. *J. Atmos. Oceanic Technol.*, 28:1373–1389, 2011a.
- Q. Lu, W. Bell, P. Bauer, N. Bormann, and C. Peubey. An evaluation of FY-3A satellite data for numerical weather prediction. *Q. J. R. Meteorol. Soc.*, 137:1298–1311, 2011b.
- X. Zhou, X. Wand, F. Weng, and G. Li. Assessments of Chinese Fengyun Microwave Temperature Sounder (MWTS) measurements for weather and climate applications. *J. Atmos. Oceanic Technol.*, 28:1206–1227, 2011.